



## Effect of transmembrane pressure on draw solution channel height and water flux in spiral wound forward osmosis module

Jongmin Jeon<sup>a</sup>, Jaehak Jung<sup>a</sup>, Joon Young Choi<sup>b</sup>, Jaebum Kim<sup>c</sup>, Suhan Kim<sup>a,\*</sup>

<sup>a</sup>Department of Civil Engineering, Pukyong National University, 45 Yongso-ro, Nam-gu, Busan 608-737, Korea, Tel. +82 51 629 6065, Fax: +82 51 629 6063; email: suhankim@pknu.ac.kr (S. Kim)

<sup>b</sup>Institute of Technology, Hyorim Industries Inc., 1161-73, Jisan-dong, Suseong-gu, Daegu, Korea

<sup>c</sup>Jeju Regional Division, Korea Institute of Industrial Technology (KITECH), 102 Jejudaehak-ro, Jeju-si, Jeju-do, Korea

Received 1 March 2017; Accepted 16 May 2017

### ABSTRACT

An 8-inch commercial spiral wound forward osmosis (FO) module was tested to investigate the effect of transmembrane pressure on the performance of the FO membrane. A coupon taken from the FO module was tested in a lab-scale FO system to determine water and solute permeability of the membrane. The positive transmembrane pressure enhances the water flux of the FO module, and interestingly the amount of the flux enhancement exceeds the multiplication of the water permeability and the transmembrane pressure. This abnormal flux enhancement is caused by the shrunken draw solution (DS) channel height, which is clearly verified by the hydraulic tests in this work. The shrunken DS channel height makes the effect of external concentration polarization smaller, which should be one of the potent reasons for the additional flux enhancement. This finding suggests that an adequate transmembrane is effective to operate FO systems using spiral wound modules to extract better performance of the modules.

**Keywords:** Forward osmosis; Spiral wound module; Draw solution channel height; Water flux enhancement

### 1. Introduction

Recently forward osmosis (FO) process has been focused on as a desalination method [1–3]. Instead of using hydraulic pressure like reverse osmosis (RO) does, FO uses osmotic pressure for filtration. Because of its low pressure characteristics, FO has more advantages than RO in terms of energy consumption and low fouling [3–7]. Currently, FO applications cover not only seawater desalination but also wider since areas such as food processing, wastewater treatment, microalgae harvesting, and so on [8–13].

Most FO studies focused on the water and salt transfer mechanisms through the FO membrane [13–17]. However, these results were based on the lab-scale experiments using a small piece of the membrane sheet, which is called as a

coupon. In a real scale FO process, FO modules should be adopted instead of coupons. Since the FO membrane area in the module is much larger than that in the coupon, the filtration phenomenon should be complicated. The feed solution (FS) is concentrated and the draw solution (DS) becomes diluted as they flow through the FO module. Therefore, the FO membrane characteristics with lab-scale experiment cannot directly indicate the performance of the FO modules.

Previous studies have been conducted to investigate factors affecting the performance of FO modules [13,18–23]. Lotfi et al. [13] tested with thin-film composite (TFC) hollow fiber module using fertilizer as DS. Kim et al. [19] tested a commercial spiral wound FO module (HTI, Albany, USA) with two different type spacers. Attarde et al. [20,21] tested a commercial spiral wound FO module (HTI, Albany, USA) and estimated the modeling results with using the experimental

\* Corresponding author.

results. Shibuya et al. [22] conducted the FO module test using a commercial cellulose triacetate (CTA) hollow fiber module (Toyobo, Japan) and compared the theoretical prediction with the experimental results. Kim et al. [23] tested two different 8" spiral wound FO modules: CTA (HTI, Albany, USA) and TFC (Toray Chemical Korea, Gumi, Korea).

In the spiral wound FO module, the FS flows in the FS channel between the enrolled layers, and the DS flows through the central tube into the inner side of the membrane enroll. Thus, flow patterns and flow resistance in the FS and DS channels should be different and influenced by characteristic module design. Recently, some studies connecting operating conditions (e.g., flow rates and inlet pressures) to resulting performances (e.g., water flux, reverse solute flux, fouling, and cleaning efficiency) of spiral wound FO modules were introduced to improve the operability of recent spiral wound FO modules in real-scale application [18–26]. These studies are of critical importance for further FO process development since the operation of spiral wound FO modules in plants is influenced by several factors such as the number of membrane leaves, FS and DS channel height, kind of spacers that influence mass transfer and pressure loss [26]. Unfortunately, these studies found that the water flux in the spiral wound FO module was much smaller than that observed in the coupon test.

In order to increase the low water flux in FO, a new FO concept named pressure-assisted osmosis (PAO) has been introduced [27–29]. In PAO, the applied pressure on the FS side of the membrane to improve the water flux through the effects of pressure and osmotic pressure [27–29]. By increasing the hydraulic pressure, the water flux was considerably enhanced despite of higher ICP [30–31]. Oh et al. [32] suggested the water flux in PAO when pure water is used as FS such as:

$$J_w = A(\Delta P + \pi_{D,b} \exp(-J_w K)) \quad (1)$$

where  $A$  is the membrane water permeability,  $\pi_{D,b}$  is the DS osmotic pressure, and  $K$  is the solute resistance to diffusion within the porous support layer. The water flux in PAO is the sum of two independent different flux components: an osmotic flux and a pressure-driven flux. As shown in Eq. (1), the increased water flux by the applied hydraulic pressure decreased the effective osmotic pressure due to enhanced ICP, which means that the amount of the flux enhancement by applying the hydraulic pressure,  $P$ , is supposed to be smaller than the multiplication of the membrane permeability,  $A$ , and  $P$ . The model based on Eq. (1) shows a good agreement with a well-controlled lab-scale FO test [32].

However, there have been few studies dealing with the mechanism of the flux enhancement by the positive transmembrane pressure (i.e., the pressure on the FS side is higher than that on the DS side.) in the module-scale study. Unlike the coupon-based experimental study, it is possible to investigate the effect of transmembrane pressure on the pressure differential of the membrane channel (i.e., the pressure difference between the inlet and outlet of the channel) in the module-size experimental study. The pressure differential can be an indicator for the change in the channel height. Therefore, this study focused on the effect of transmembrane

pressure on the DS channel height and its relation to water flux enhancement in spiral wound FO module.

## 2. Methods

### 2.1. Lab-scale experiment

Lab-scale experiment was carried out to determine water and solute permeability ( $A$  and  $B$ ) of the FO membrane. A TFC FO membrane coupon was taken from the FO8040 spiral wound module (Toray Chemical Korea, Inc). The lab-scale FO system is described in Fig. 1. The FO cells have two identical channels on both sides of the membrane for the FS and DS. The channel dimensions are 0.11 m in length, 0.06 m in width, and 0.001 m in height. Thus, the membrane surface area and cross-sectional area are  $6.6 \times 10^{-3}$  and  $6.0 \times 10^{-5}$  m<sup>2</sup>, respectively. Spacers were installed within both channels to enhance the support of the FO membrane as well as the solute mass transfer by causing turbulence.

Sodium chloride (NaCl) from industrial refined salt (OCI Co. Ltd., China) was used as DS. The water and reverse solute flux ( $J_w$  and  $J_s$ ) were measured during the lab-scale experiment. Cross-flow velocities of FS and DS sides were set at  $0.25 \text{ m s}^{-1}$  by the two identical gear pumps (longer pump WT3000-1FA). The FO experiment started with deionized water of the same temperature ( $18^\circ\text{C}$ ) on FS and DS sides. Then, the DS side is changed with the DS of the demanded salt concentration in the range of 0.25–1 M as NaCl. When a steady state was reached, permeate water flux ( $J_w$ ) can be calculated by weighing DS.

The salt concentration in the FS was also measured in 3 min intervals and the reverse solute flux ( $J_s$ ) was calculated from the change of salt concentration in the feed using the following equation:

$$J_s = \frac{C_{f,t}(V_{f0} - J_w A_m t)}{A_m t} \quad (2)$$

where  $t$ ,  $C_{f,t}$ ,  $V_{f0}$  and  $A_m$  are the elapsed filtration time, salt concentration in feed at time  $t$ , the initial volume of FS, and membrane area, respectively. The experimentally measured water and reverse solute flux were used to determine the

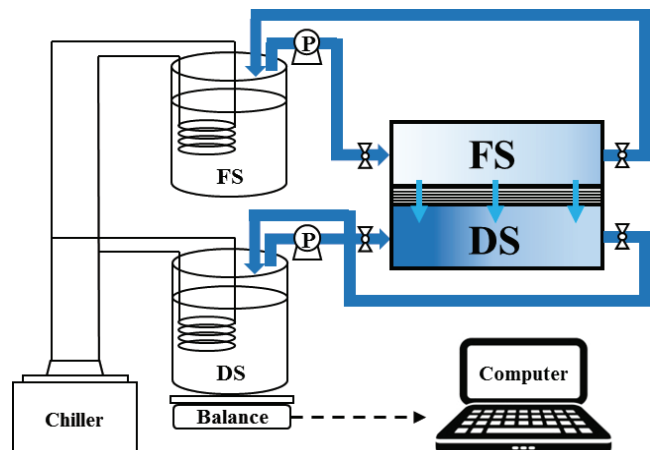


Fig. 1. Schematic diagram of FO lab-scale tester.

water and solute permeability of the tested FO membrane based on the methodology introduced in a recent literature published by our research group [17].

2.2. FO module experiment

For the FO flux test using the spiral wound module, FS and DS concentrations were initially set to 0 and 1 M as NaCl. The FS and DS flow rates, and transmembrane pressure were set to a desired value by controlling valves in the FO module test described in Fig. 2.

DS and FS flowed into the tested FO module and returned to their own tanks, which results in diluting DS and concentrating FS during the test. The volume of each tank is 400 L. FS flow rate ( $Q_f$ ), concentrate flow rate ( $Q_c$ ), feed concentration ( $C_f$ ), concentrate concentration ( $C_c$ ), DS flow rate ( $Q_d$ ), and DS concentration ( $C_d$ ) can be observed in real time. Pressure gauges are located at the inlet and outlet of both channels. Input flow rates to the module ( $Q_f$  and  $Q_d$ ) are adjusted by valves. The diluted DS flow rate ( $Q_{dd}$ ) and concentration ( $C_{dd}$ ) can be calculated using equation based on the mass balance inside the module:

$$Q_{dd} = Q_d + (Q_f - Q_c) \tag{3}$$

$$C_{dd} = \frac{(Q_d C_d + Q_f C_f - Q_c C_c)}{Q_{dd}} \tag{4}$$

The average water flux of FO module ( $J_w$ ) is determined by:

$$J_w = \frac{Q_f - Q_c}{A_m} \tag{5}$$

where  $A_m$  is total membrane surface area of the module.  $J_s$  is calculated based on the mass balance inside the FS channel given as follows:

$$J_s = \frac{(Q_c C_c - Q_f C_f)}{A_m} \tag{6}$$

where we neglected the rejection rate of salts in FS by FO membrane and only considered the reverse solute flux from

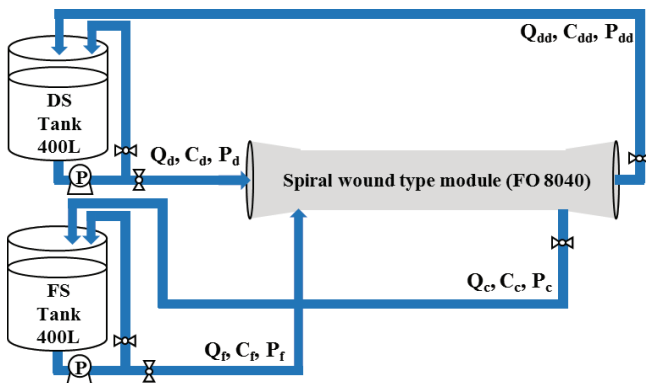


Fig. 2. Schematic diagram of FO module tester.

DS to FS because only one solute, sodium chloride is used in this work.

In order to investigate the relationship between the DS channel height and the transmembrane pressure, hydraulic tests were carried out with FO module tester. The hydraulic test started with pure water of the same temperature (18°C) on the FS and DS tanks. The pure water was provided by a bench-scale reverse osmosis (RO) system with tap water as RO feed and a 4-inch seawater RO membrane (RE4040-SHN, Toray Chemical Korea). Sodium bisulfite was used to the tap water to remove free chlorine from tap water to preserve the polyamide RO membrane. The hydraulic tests were performed in various combinations of the FS and DS flow rates and transmembrane pressures. The inlet and outlet pressures of the FS and DS channel were measured to calculate transmembrane pressure and pressure differential during the tests. The negative transmembrane was avoided because it can damage the glue line of the DS channel in the spiral wound FO module.

3. Results and discussion

3.1. FO membrane properties

Water and solute permeability ( $A$  and  $B$ ) are two main properties of an FO membrane. As discussed in section 2, we determined  $A$  and  $B$  values by the FO method developed in our previous study [17]. For the FO method, an FO membrane coupon of the spiral wound module was tested and both water and solute flux ( $J_w$  and  $J_s$ ) data were obtained. First,  $A$  is determined to minimize the errors between the experimental and modeling data for water flux as shown in Fig. 3(a). The determined value for  $A$  is  $1.65 \times 10^{-11} \text{ m s}^{-1} \text{ Pa}^{-1}$  at 18°C. Once  $A$  is obtained,  $B$  is calculated using the relationship between  $A$  and  $B$ , such as:

$$B = (J_s / J_w) \beta R_g T A \tag{7}$$

where the value of  $J_s / J_w$  can be calculated using water and solute flux obtained experimentally;  $\beta$  is the van't Hoff coefficient (e.g.,  $\beta = 2$  for NaCl);  $R_g$  is the universal gas constant; and  $T$  is the absolute temperature [17]. Fig. 3(b) shows the experimental and modeling data for solute flux, where the modeling data were calculated by Eq. (7) using the determined  $B$  value ( $=4.26 \times 10^{-7} \text{ m s}^{-1}$ ). The experimental solute flux matches the modeling value fairly well. The match between the experimental and modeling data shown in Fig. 3 means that the determined  $A$  and  $B$  values can express the FO membrane characteristics very well. The determined  $A$  value is used to analyse the effect of transmembrane pressure on the water flux of the spiral wound FO membrane module, which will be explained in section 3.2.

3.2. Effect of transmembrane pressure on water flux of the spiral wound FO module

Fig. 4(a) shows the water flux data of the spiral wound FO module as a function of DS concentration when transmembrane pressure exists or not. The water flux in the module is smaller than that observed in the coupon test as shown in

Figs. 3(a) and 4(a). In the module, the osmotic pressure difference between DS and FS decreases because DS and FS are diluted and concentrated, respectively. In addition, the effect of module shape on the DS and FS flow (e.g., dead-zone and uneven flow distribution) may prevent DS from drawing water out of FS.

As shown in Fig. 4(a), the operation with transmembrane pressures of 0.69–0.91 bar results in higher water flux than the FO operation without transmembrane pressure. The water flux difference ranges from 8.8 to 9.9 LMH. In both cases where transmembrane pressure is exerted or not, the water flux increases at higher DS concentrations because the osmotic pressure difference between DS and FS increases. In the case of zero transmembrane pressure, the duplicate module tests were carried out to find out whether the experimental results were reproducible or not.

The most suspected reason for the water flux difference observed in Fig. 4(a) is the increased water flux by transmembrane pressure (i.e.,  $A\Delta P$ ), which is linearly proportional to the water permeability of FO membrane,  $A$ . Thus, it is compared with the actual water flux difference ( $\Delta J_w$ ) between the cases with and without transmembrane pressure as shown in Fig. 4(b). Interestingly,  $A\Delta P$  is smaller than  $\Delta J_w$ , which means that the increased water flux by transmembrane pressure ( $A\Delta P$ ) is not enough to explain the reason why the existence of transmembrane pressure raises the water flux. What

are other possible reasons why the water flux is enhanced by transmembrane pressure in the spiral wound FO module? If the transmembrane pressure is positive, the pressure in the FS side is higher than that in the DS side. Thus, there is a chance that the DS channel is compressed by the positive transmembrane pressure, which makes the DS channel height shrunken, which will be discussed in the next section.

### 3.3. Effect of transmembrane pressure on the DS channel height

In order to find out if the DS channel height in the spiral wound FO module is shrunken by the positive transmembrane pressure, we have collected the pressure differential data in the DS channel with various cross-flow velocities and transmembrane pressures. Fig. 5 shows the pressure differential ( $\Delta P_d$ ) in the DS channel as a function of the cross-flow velocity ( $U_{d,avg}$ ), which is the average of the inlet and outlet cross-flow velocity values in the DS channel. For the FO module experiments to obtain the results in Fig. 5, pure water was used to make FS and DS in order to avoid water flux by osmotic pressure difference between FS and DS. As shown in Fig. 5(a), the pressure differential data exhibits a scattered pattern over a second-order regression curve

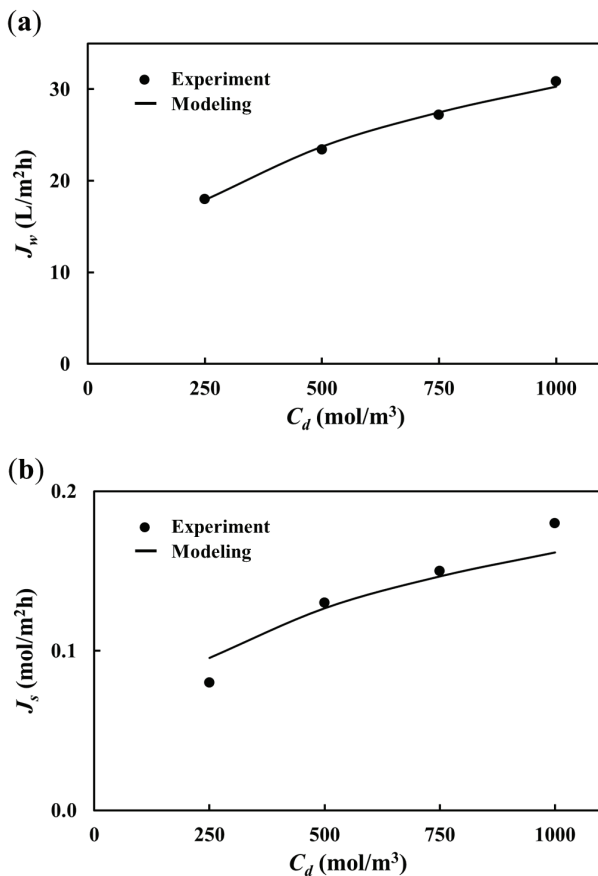


Fig. 3. The comparison between the experimental and modeling data: (a) water flux and (b) solute flux.

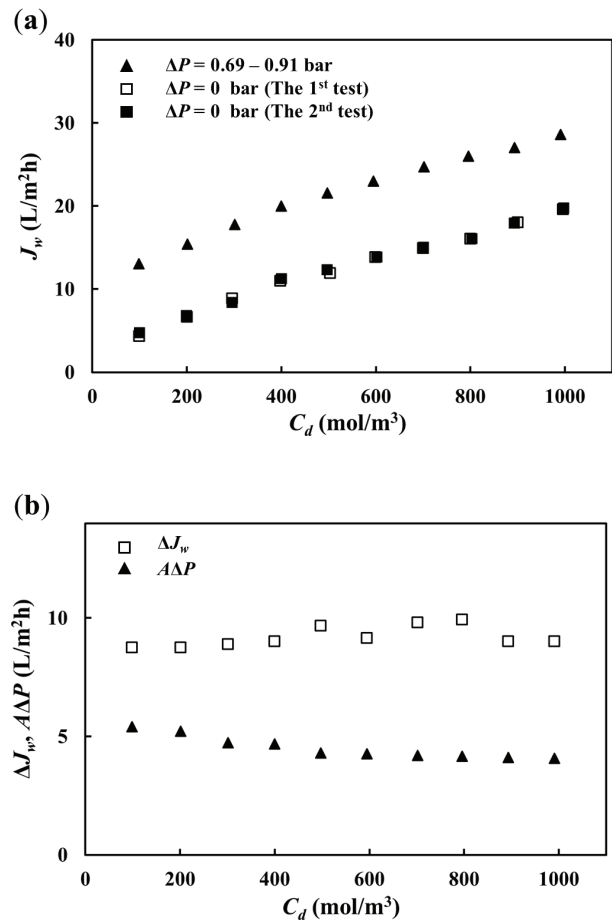


Fig. 4. Effect of transmembrane pressure on water flux in the spiral wound FO module: (a) water flux data as a function of DS concentration with/without transmembrane pressure, and (b) the comparison between water flux difference ( $=\Delta J_w$ ) in (a) and pure water flux due to transmembrane pressure ( $A\Delta P$ ).

( $R^2 = 0.97$ ). In Fig. 5(b), the  $\Delta P_d$  data were categorized into the three groups according to the transmembrane pressure range (e.g.,  $\Delta P = 0\text{--}0.9$  bar,  $1\text{--}1.9$  bar, and  $2\text{--}2.9$  bar). As a result, the categorized  $\Delta P_d$  data are well arranged over the corresponding second-order regression line, which means the transmembrane pressure ( $\Delta P$ ) should play an important role to determine pressure differential ( $\Delta P_d$ ) in the DS channel.

Eq. (7) is a linear regression model for  $\Delta P_d$  with one independent variable, the square of the average cross-flow velocity in the DS channel ( $U_{d,avg}^2$ ) and the model equation is obtained using Microsoft Excel 2010:

$$\Delta P_d = 0.0192U_{d,avg}^2 + 0.0921 \quad (R^2 = 0.952) \quad (8)$$

We can make a better regression model in terms of the coefficient of determination ( $R^2$ ) by introducing another independent variable, the transmembrane pressure ( $\Delta P$ ) such as:

$$\Delta P_d = 0.0213U_{d,avg}^2 + 0.135\Delta P + 0.0458 \quad (R^2 = 0.974) \quad (9)$$

where the p value for  $\Delta P$  is  $1.41 \times 10^{-6}$ , which means the probability that the coefficient of  $\Delta P$  becomes zero is extremely low, and thus  $\Delta P$  should affect the change in  $\Delta P_d$ . In Eq. (8), the coefficient of  $\Delta P$  is positive (e.g., 0.135), which means the positive transmembrane pressure causes the increase in  $\Delta P_d$ .

The higher the transmembrane pressure ( $\Delta P$ ) is, the higher pressure differential in the DS channel ( $\Delta P_d$ ) becomes. This pattern is clearly described in Fig. 5(b) and in the positive coefficient of  $\Delta P$  in Eq. (8) as well. The pressure differential in a closed channel changes when cross-flow velocity or channel dimension is changed. If the cross-flow rate, length, width, and friction factor of the DS channel are maintained constantly, the increase in the pressure differential can be explained by the decrease in the DS channel height. This hypothesis is well supported by the fact that the transmembrane pressure perpendicular to FO membrane surface should not affect the changes in the friction factor, the width and length of the DS channel. If the DS channel height is shrunken by the positive transmembrane pressure, the abnormal flux increase observed in Fig. 4(b) (i.e.,  $\Delta J_w > A\Delta P$ ) can be related to the decreased external concentration polarization (ECP) due to the increased cross-flow velocity by the shrunken DS channel height with the same cross-flow rate as explained in Fig. 6.

#### 4. Conclusions

In this work, the effect of the transmembrane pressure on the DS channel height and water flux in spiral wound FO module was investigated. The increase in transmembrane pressure results in the flux enhancement of the FO module, and interestingly, it exceeds the expected flux enhancement calculated by the multiplication between the water permeability and the transmembrane pressure. One of the potent reasons for this abnormal flux enhancement is the shrunken DS channel height due to the applied hydraulic pressure, which is clearly verified by the hydraulic tests using the FO module. The shrunken DS channel height makes the ECP effect smaller and the flux higher. Using this finding, it is suggested to operate the real-scale FO system with an adequate transmembrane pressure to compensate the performance of the FO module in the system.

#### Acknowledgments

This research was supported by a grant (code 171FIP-B088091-04) from Industrial Facilities and Infrastructure Research Program funded by Ministry of Land, Infrastructure and Transport of Korean government.

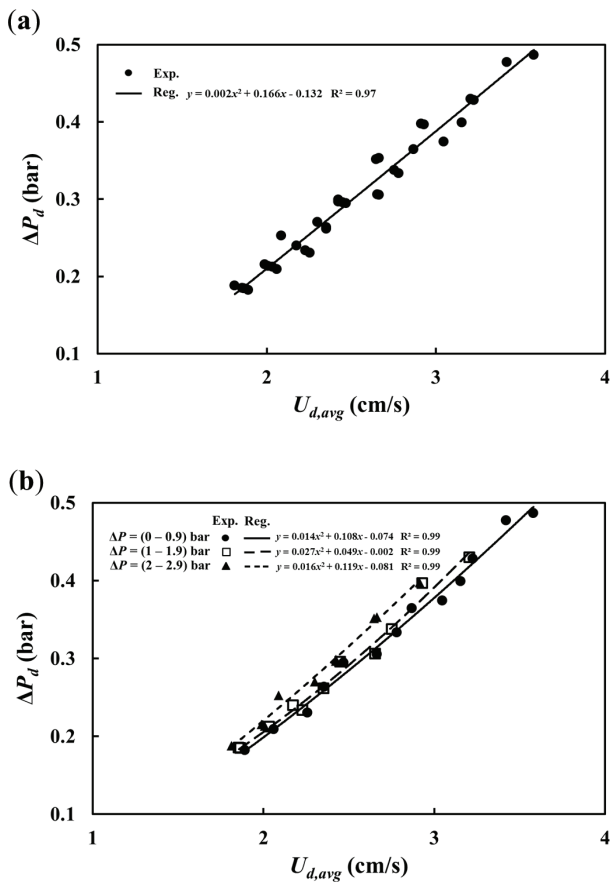


Fig. 5. The pressure differential ( $\Delta P_d$ ) in the DS channel as a function of the average cross-flow velocity ( $U_{d,avg}$ ) in the channel (Exp. and Reg. mean experimental and the regression model data, respectively).

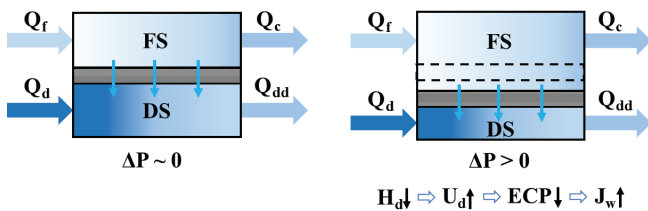


Fig. 6. The conceptual schematic for the effect of positive transmembrane pressure on the permeate flux in the spiral wound FO module.

## References

- [1] T.Y. Cath, A.E. Childress, M. Elimelech, Forward osmosis: principles, applications, and recent developments, *J. Membr. Sci.*, 281 (2006) 70–87.
- [2] J.R. McCutcheon, M. Elimelech, Modeling water flux in forward osmosis: implications for improved membrane design, *AIChE J.*, 53 (2007) 1736–1744.
- [3] J.R. McCutcheon, M. Elimelech, Influence of concentrative and dilutive internal concentration polarization on flux behavior in forward osmosis, *J. Membr. Sci.*, 284 (2006) 237–247.
- [4] M. Elimelech, W.A. Phillip, The future of seawater desalination: energy, technology, and the environment, *Science*, 333 (2011) 712–717.
- [5] B. Mi, M. Elimelech, Organic fouling of forward osmosis membranes: fouling reversibility and cleaning without chemical reagents, *J. Membr. Sci.*, 348 (2010) 337–345.
- [6] Y.-J. Choi, J.-S. Choi, H.-J. Oh, S. Lee, D.R. Yang, J.H. Kim, Toward a combined system of forward osmosis and reverse osmosis for seawater desalination, *Desalination*, 247 (2009) 239–246.
- [7] J. Jeon, B. Park, Y. Yoon, S. Kim, An optimal design of forward osmosis and reverse osmosis hybrid process for seawater desalination, *Desal. Wat. Treat.*, 57 (2016) 26612–26620.
- [8] S.H. Park, B. Park, H.K. Shon, S. Kim, Modeling full-scale osmotic membrane bioreactor systems with high sludge retention and low salt concentration factor for wastewater reclamation, *Bioresour. Technol.*, 190 (2015) 508–515.
- [9] S. Kim, Scale-up of osmotic membrane bioreactors by modelling salt accumulation and draw solution dilution using hollow-fiber membrane characteristics and operation conditions, *Bioresour. Technol.*, 165 (2014) 88–95.
- [10] S. Kim, S. Paudel, G.T. Seo, Forward osmosis membrane filtration for microalgae harvesting cultivated in sewage effluent, *Environ. Eng. Res.*, 20 (2015) 99–104.
- [11] S. Zhao, L. Zou, C.Y. Tang, D. Mulcahy, Recent developments in forward osmosis: opportunities and challenges, *J. Membr. Sci.*, 396 (2012) 1–21.
- [12] S. Zou, Y. Gu, D. Xiao, C.Y. Tang, The role of physical and chemical parameters on forward osmosis membrane fouling during algae separation, *J. Membr. Sci.*, 366 (2011) 356–362.
- [13] F. Lotfi, S. Phuntsho, T. Majeed, K. Kim, D.S. Han, A.A.-Wahab, H.K. Shon, Thin film composite hollow fibre forward osmosis membrane module desalination of brackish groundwater for fertigation, *Desalination*, 364 (2015) 108–118.
- [14] J. Lee, S. Kim, Predicting power density of pressure retarded osmosis (PRO) membranes using a new characterization method based on a single PRO test, *Desalination*, 389 (2016) 224–234.
- [15] R. Wang, L. Shi, C.Y.Y. Tang, S.R. Chou, C. Qiu, A.G. Fane, Characterization of novel forward osmosis hollow fiber membranes, *J. Membr. Sci.*, 355 (2010) 158–167.
- [16] G.T. Gray, J.R. McCutcheon, M. Elimelech, Internal concentration polarization in forward osmosis: role of membrane orientation, *Desalination*, 197 (2006) 1–8.
- [17] J. Lee, J.Y. Choi, J.-S. Choi, K.H. Chu, Y. Yoon, S. Kim, A statistics-based forward osmosis membrane characterization method without pressurized reverse osmosis experiment, *Desalination*, 403 (2017) 36–45.
- [18] J. Jeon, J. Jung, J.Y. Choi, S. Kim, The performance of the spiral wound and flat sheet forward osmosis elements with thin film composite membrane, *Desal. Wat. Treat.* (in press).
- [19] J.E. Kim, S. Phuntsho, F. Lotfi, H.K. Shon, Investigation of pilot-scale 8040 FO membrane module under different operating conditions for brackish water desalination, *Desal. Wat. Treat.*, 53 (2015) 2782–2791.
- [20] D. Attarde, M. Jain, S.K. Gupta, Modeling of a forward osmosis and a pressure-retarded osmosis spiral wound module using the Spiegler-Kedem model and experimental validation, *Sep. Purif. Technol.*, 164 (2016) 182–197.
- [21] D. Attarde, M. Jain, K. Chaudhary, S.K. Gupta, Osmotically driven membrane processes by using a spiral wound module – modeling, experimentation and numerical parameter estimation, *Desalination*, 361 (2015) 81–94.
- [22] M. Shibuya, M. Yasukawa, S. Goda, H. Sakurai, T. Takahashi, M. Higa, H. Matsuyama, Experimental and theoretical study of a forward osmosis hollow fiber membrane module with a cross-wound configuration, *J. Membr. Sci.*, 504 (2016) 10–19.
- [23] J.E. Kim, G. Blandin, S. Phuntsho, A. Verliefde, P. Le-Clech, H.K. Shon, Practical considerations for operability of an 8" spiral wound forward osmosis module: hydrodynamics, fouling behaviour and cleaning strategy, *Desalination*, 404 (2017) 249–258.
- [24] Y.C. Kim, S.J. Park, Experimental study of a 4040 spiral-wound forward-osmosis membrane module, *Environ. Sci. Technol.*, 45 (2011) 7737–7745.
- [25] R.L. McGinnis, N.T. Hancock, M.S. Nowosielski-Slepowron, G.D. McGurgan, Pilot demonstration of the NH<sub>3</sub>/CO<sub>2</sub> forward osmosis desalination process on high salinity brines, *Desalination*, 312 (2012) 67–74.
- [26] J. Schwinge, P.R. Neal, D.E. Wiley, D.F. Fletcher, A.G. Fane, Spiral wound modules and spacers: review and analysis, *J. Membr. Sci.*, 242 (2004) 129–153.
- [27] G. Blandin, A.R. Verliefde, P. Le-Clech, Pressure enhanced fouling and adapted antifouling strategy in pressure assisted osmosis (PAO), *J. Membr. Sci.*, 493 (2015) 557–567.
- [28] G. Blandin, A.R.D. Verliefde, C.Y. Tang, A.E. Childress, P. Le-Clech, Validation of assisted forward osmosis (AFO) process: impact of hydraulic pressure, *J. Membr. Sci.*, 447 (2013) 1–11.
- [29] S. Sahebi, S. Phuntsho, J.E. Kim, S. Hong, H.K. Shon, Pressure assisted fertiliser drawn osmosis process to enhance final dilution of the fertiliser draw solution beyond osmotic equilibrium, *J. Membr. Sci.*, 481 (2015) 63–72.
- [30] J. Duan, E. Litwiller, I. Pinnau, Solution-diffusion with defects model for pressure assisted forward osmosis, *J. Membr. Sci.*, 470 (2014) 323–333.
- [31] S. Jamil, S. Jeong, S. Vigneswara, Application of pressure assisted forward osmosis for water purification and reuse of reverse osmosis concentrate from a water reclamation plant, *Sep. Purif. Technol.*, 171 (2016) 182–192.
- [32] Y. Oh, S. Lee, M. Elimelech, S. Lee, S. Hong, Effect of hydraulic pressure and membrane orientation on water flux and reverse solute flux in pressure assisted osmosis, *J. Membr. Sci.*, 465 (2014) 159–166.